Université de Mons
Faculté Polytechnique – Service de Mécanique Rationnelle, Dynamique et Vibrations
31, Bld Dolez - B-7000 MONS (Belgique)
065/37 42 15 – georges.kouroussis@umons.ac.be

J. Yang, S. Zhu, W. Zhai, G. Kouroussis, Y. Wang, K. Wang, K. Lan, F. Xu, Prediction and mitigation of train-induced vibrations of large-scale building constructed on subway tunnel, *Science of the Total Environment*, 668: 485–499, 2019.

Science of the Total Environment 668 (2019) 485–499

Contents lists available at ScienceDirect

Science of the Total Environment

journal homepage: www.elsevier.com/locate/scitotenv

Prediction and mitigation of train-induced vibrations of large-scale building constructed on subway tunnel

Jianjin Yang [a], Shengyang Zhu [a,*], Wanming Zhai [a], Georges Kouroussis [b], Yue Wang [c], Kaiyun Wang [a], Kai Lan [c], Fangzheng Xu [a]

[a] Train and Track Reasearch Institute, State Key Laboratory of Traction Power, Southwest Jiaotong University, Chengdu, China
[b] Department of Theoretical Mechanics, Dynamics and Vibrations, University of Mons, Mons, Belgium
[c] Sichuan Province Airport Group Co., Ltd., Chengdu, China

HIGHLIGHTS

- Underground train-induced vibrations are considered.
- Virtual prototyping is an efficient tool to analyse ground-borne vibrations.
- A prediction scheme is used to calculated vibrations in large-scale building.
- VAL and VALIF indicators are used for analyzing the structural vibrations.
- Mitigation measures are brought by anti-seismic base isolations.

GRAPHICAL ABSTRACT

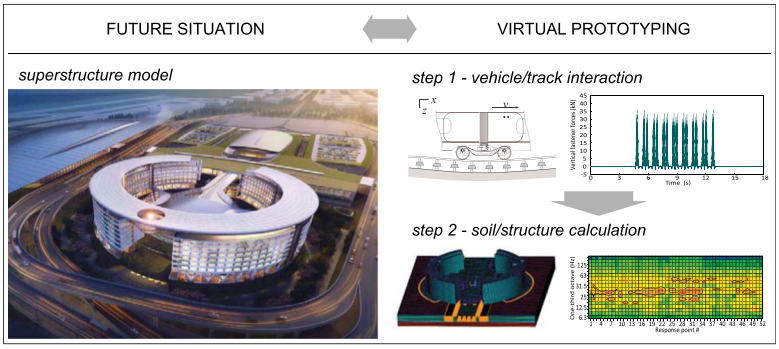

ARTICLE INFO

Article history:
Received 25 December 2018
Received in revised form 16 February 2019
Accepted 25 February 2019
Available online 01 March 2019

Editor: Pavlos Kassomenos

Keywords:
Environmental impact assessment (EIA)
Train-induced vibrations
Large-scale building vibration
Subway network
Rail track vibration mitigation
Building virtual prototyping

ABSTRACT

Among all the recent improvements in the railway industry, ground vibration remains an important showstopper in metropolitan cities. In some particular cases, significant levels of vibration are felt by residents. The role of engineers is to propose mitigation solutions and to ensure that they are efficient in the long-term. This paper presents a numerical study of a large-scale building close to underground networks. A two-step time-frequency prediction method for train-induced vibrations of a superstructure is proposed in this work. In the first step, the spatial train-track coupled dynamic model in time domain is established and then simulated to obtain the vertical and lateral rail supporting forces (fastener forces). In the second step, the discrete Fourier Transform (DFT) of fastener forces are taken as the external loads of a finite element (FE) model of the track-tunnel-soil-building system to solve the building vibrations. On this basis, train-induced vibrations of the large-scale building are predicted under different train operation conditions, and two relevant standards are adopted to evaluate the building vibrations. Further, a base isolation measure, that consists in installing steel springs between the superstructure and the base, is employed to mitigate excessive building vibration. Results show that the underground train and track interaction could result in over-limit building vibrations. The train moving with a higher speed will deteriorate track vibration level and leads to more serious extent of over-limit vibrations of the larger-scale building. The base isolation measure can effectively reduce the excessive building vibrations, and also ensures the train-induced vibrations of the building to satisfy the relevant standard requirements under the worst train operation conditions.

* Corresponding author.
E-mail address: syzhu@swjtu.edu.cn (S. Zhu).

https://doi.org/10.1016/j.scitotenv.2019.02.397
0048-9697/

1. Introduction

The urban railway traffic is an important part of urban transport system and even one of the strategic vectors for the development of metropolitan cities, due to its advantages such as large transport capacity, high velocity, energy conservation, environment protection, as well as safety and punctuality. Despite these benefits, some issues associated to its implementation and operation must be considered. Among this range of issues, the vibrations induced by the train running on the track, propagating through the surrounding soil to the ground and the buildings in the vicinity of the track, became a main cause of annoyance of occupant comfort (Thompson, 2009; Kouroussis et al., 2014a; Connolly et al., 2016; Zhu et al., 2017; Zhang et al., 2018). Thus, it is extremely important to study the vibrations induced by railway traffic.

Over the past three decades, the industrial and scientific community has paid a special attention to this issue and several prediction models have been developed for the train-induced ground vibration prediction, ranging from scoping and empirical rules (Madshus et al., 1996; Verbraken et al., 2011; Connolly et al., 2014) to analytical and semi-analytical models (Sheng et al., 2004; Hussein and Hunt, 2007), without forgetting complex numerical models, as the ones suggested by Lombaert and Degrande (2001), Clouteau et al. (2005), Degrande et al. (2006), Gupta et al. (2009), Galvin et al. (2010), Hung and Yang (2010) and Kouroussis and Verlinden (2013), among others. These methods are quite useful, due to their potential in identification of the key parameters involved in the phenomenon as well as their influences (Lopes et al., 2014a; Kouroussis et al., 2014b; Vogiatzis and Kouroussis, 2015). Nevertheless, the application of these models still presents some limitations from a practical point of view, due to their difficulty in simulating real scenarios with complex configurations and variegated dynamic characteristics.

The development and usage of the aforementioned models and methods assured a better understanding of the phenomena of generation and propagation of train-induced ground vibration. In terms of the building vibration induced by the railway traffic, the common methods are experimental (Xia et al., 2005, 2009; Masoud et al., 2014; Lopes et al., 2014b; Zou et al., 2015, 2017; Vogiatzis et al., 2018) and numerical (Coulier et al., 2014; Hunt, 1996; Santos et al., 2017). The experimental methods can obtain the effective vibrations of the building under realistic conditions (Lopes et al., 2016; Vogiatzis et al., 2018); however, they are difficult to implement before the urban railway traffic is in operation. In some numerical methods, the ground vibrations are firstly calculated using prediction methods for ground vibration and then the ground vibrations are input into the soil-structure dynamic interaction models to acquire the building vibrations.

For the purpose of saving land cost and bringing more convenient trips, the urban railway is co-constructed with the buildings (Zou et al., 2015, 2017). In this case, the compound numerical prediction models are not available, because the vibrations transmitted to the building through the shared structure between the railway and the building could be more serious than that through the soil. Combined with an engineering practice, this paper proposes a feasible prediction model which is available even in various circumstances. Usually, a hotel is planned to be built close to an airport (shown in Fig. 1) and metro lines will connect the airport with the urban districts. Due to limited space and convenience for travelers, the hotel will be built above a tunnel. The tunnel is used for access roads to the airport and two metro lines. Parts of the hotel are directly supported on the tunnel through pillars (shown in Fig. 2), therefore the vibrations could propagate to the structures of the hotel through the soil as well as the pillars. The hotel is composed of the main building and the podium building which are structurally connected. The main building shape is cylindrical and includes two parts both of which are eight-floor buildings. In order to resist to earthquake and to limit the structural deformation, there is a gap in each eight-floor building. The main building is a large-scale structure that is mainly used for accommodation purposes. The podium building is a two-floor building which is mainly used for office use. Generally speaking, the hotel is almost symmetrical about the vertical mid-plane of the tunnel in the longitudinal direction. The research focus of this paper will be put on the train-induced vibration of the main building.

To quantify the effect of vibration and to assess the efficiency of possible mitigation solutions prior to construction, a prediction model is built, classifying the present research work as a virtual prototyping. Firstly, a two-step time-frequency prediction method for the train-induced vibration of the large-scale building is proposed. In the first step, the spatial train-track coupled dynamic model is established in time domain to obtain the vertical and lateral rail supporting force (fastener forces). In the second step, the discrete Fourier transform (DFT) of

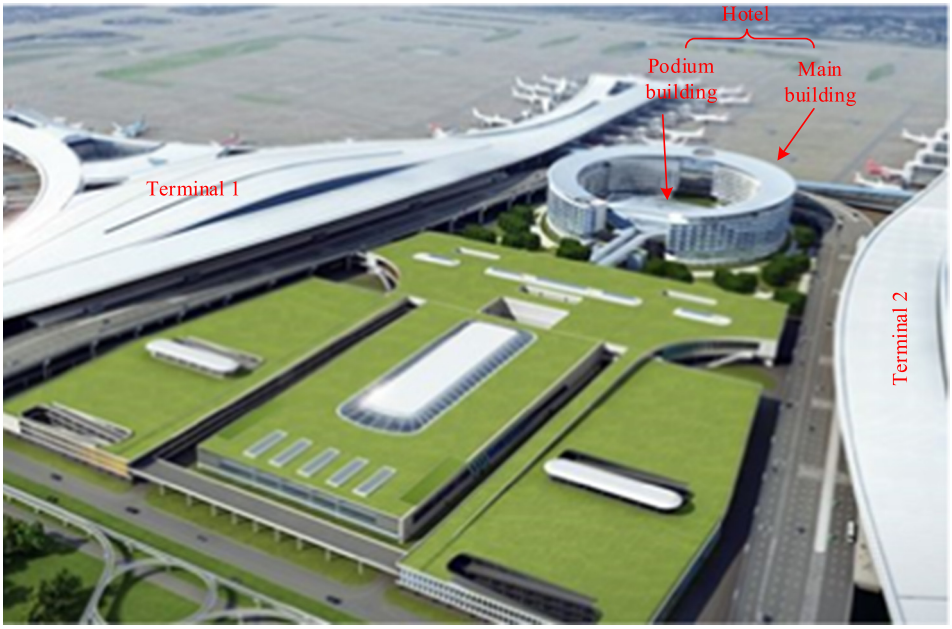

Fig. 1. Hotel built in the airport.

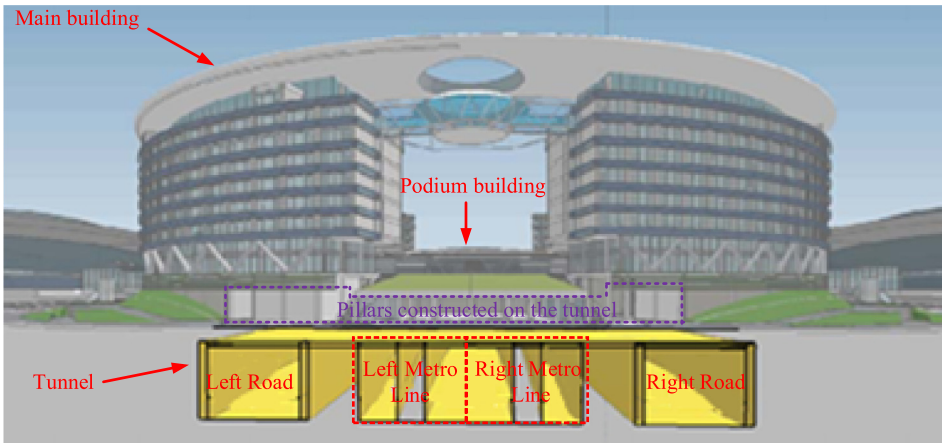

Fig. 2. Hotel co-constructed with the subway tunnel.

fastener forces is used to define the external loads of the finite element (FE) model of track-tunnel-soil-building system to solve the building vibration. Then two relevant Chinese standards, close to the international standard ISO2631-1-1997, are used to evaluate the building vibration. Finally, the base isolation measure is adopted to control the over-limit building vibration induced by underground train, and its vibration isolation effect is analyzed.

2. Prediction method

In the first step, a spatial train-track dynamic interaction model in time domain is established based on vehicle-track coupled dynamics theory (Zhai et al., 1996; Zhai et al., 2009; Zhai et al., 2013; Cai et al., 2019), which has been verified and applied to a large number of engineering problems. In the spatial train-track dynamic interaction model, a dynamic wheel/rail interaction model (Chen and Zhai, 2004) is adopted, including the rail and wheel geometric irregularities in the excitation mechanism.

In the second step, the track, the tunnel, the soil and the building are elaborately modelled using the finite element method, and are coupled through the deformation compatibility conditions at the interfaces to form a FE dynamic model of track-tunnel-soil-building coupling system. The detailed geometry and the layering of the building and the soil are fully considered in the FE model.

These two simulation steps are correlated by the fastener forces, forming the two-step numerical methodology. In the first step, the time-domain fastener forces are obtained using the spatial train-track coupled dynamic model without considering the influence of the deformations of the embankment and the soil. In fact, the influence of the deformations of the embankment and the soil on the fastener forces is quite small. In the second step, the fastener forces are taken as the external loads of the FE model, working in the frequency domain (a discrete Fourier transform – DFT – of the input forces is thus necessary). This correlation technique is similar to authors' previous works (Han and Zhai, 2011; Shao et al., 2013; Kouroussis et al., 2012). The Framework of the prediction methodology is illustrated in Fig. 3.

2.1. Train-track coupled dynamic model

When a train is moving on the track, the train will induce vibration of the track that dynamically impacts the track structure. The vibration of the track structure will cause the changes of the wheel/rail contact geometry and thus wheel/rail interactive forces. If the wheel/rail forces vary, the dynamic behavior of the train system will be affected. Obviously, the train and the track are essentially coupled with each other through the wheel/rail interaction (Zhai et al., 1996; Zhai et al., 2009). The train is formed by motor vehicles and trailer vehicles. Both the motor vehicles and the trailer vehicles have the similar structure. Thus the vehicle-track coupled model is the theoretical foundation for analyzing the train-track interaction. Based on the vehicle-track coupled dynamics theory (Zhai et al., 1996; Zhai et al., 2009), a spatial coupled dynamic model of the train and a floating-slab track (FST) is established in this paper, as illustrated in Fig. 4. The entire model is composed of the vehicle subsystem and the FST subsystem which are dynamically interacting via wheel/rail interactive forces.

The vehicle subsystem is composed of seven components and two suspension systems. The components include a car body, two bogie frames and four wheelsets. The suspension elements are divided into the primary and secondary suspension systems. The car body is supported by two bogie frames through the secondary suspension system and each bogie frame is connected with two wheelsets by the primary suspension system. Both suspension systems are constituted by springs and dampers that have nonlinear properties. By ignoring the interaction between the consecutive vehicles, all components are regarded as rigid bodies with five degrees of freedom (DOFs) including the bounce, lateral, roll, pitch and yaw motions. In total, each vehicle model has 35 DOFs, as listed in Table 1. Both suspension systems are modelled as spring-damper elements. The suspension forces and equations of motion of each vehicle component refer to the previous works (Zhai et al., 2009; Zhai et al., 2013). In summary, the equations of motion of each vehicle can be written in a matrix form set of second-order differential equations in the time domain:

$$\mathbf{M}_V\ddot{\mathbf{Z}}_V + \mathbf{C}_V\left(\dot{\mathbf{Z}}_V\right)\dot{\mathbf{Z}}_V + \mathbf{K}_V(\mathbf{Z}_V)\mathbf{Z}_V = \mathbf{F}_v\left(\mathbf{Z}_V, \mathbf{Z}_T, \dot{\mathbf{Z}}_V, \dot{\mathbf{Z}}_T\right) + \mathbf{F}_{EXT} \quad (1)$$

where $\mathbf{Z}_V$ and $\mathbf{Z}_T$ present the displacement vectors of the vehicle and track, respectively. $\mathbf{C}_V$ and $\mathbf{K}_V$ are the damping and stiffness matrices, which are relevant to the displacements, and velocities of the vehicle. $\mathbf{M}_V$ is the mass of the vehicle, while $\mathbf{F}_{EXT}$ describes external forces including gravitational forces and forces resulting from the centripetal acceleration when the vehicle is running through a curve track. $\mathbf{F}_V$ is the load vector involving the lateral and vertical wheel/rail forces which are deduced from the displacements and velocities of the vehicle and track.

The FST subsystem is composed of two rails and the floating slabs. The rails are fixed on the slabs by fasteners and the slabs are supported by steel springs. Both fasteners and steel springs are modelled using linear spring-damper elements. The deformation of the track base is ignored since it is quite small. Under the action of vertical and lateral wheel/rail forces, vibrations of the rails and the slabs occur. Each rail is described by a vertical motion Z_r, a lateral motion Y_r and a torsional

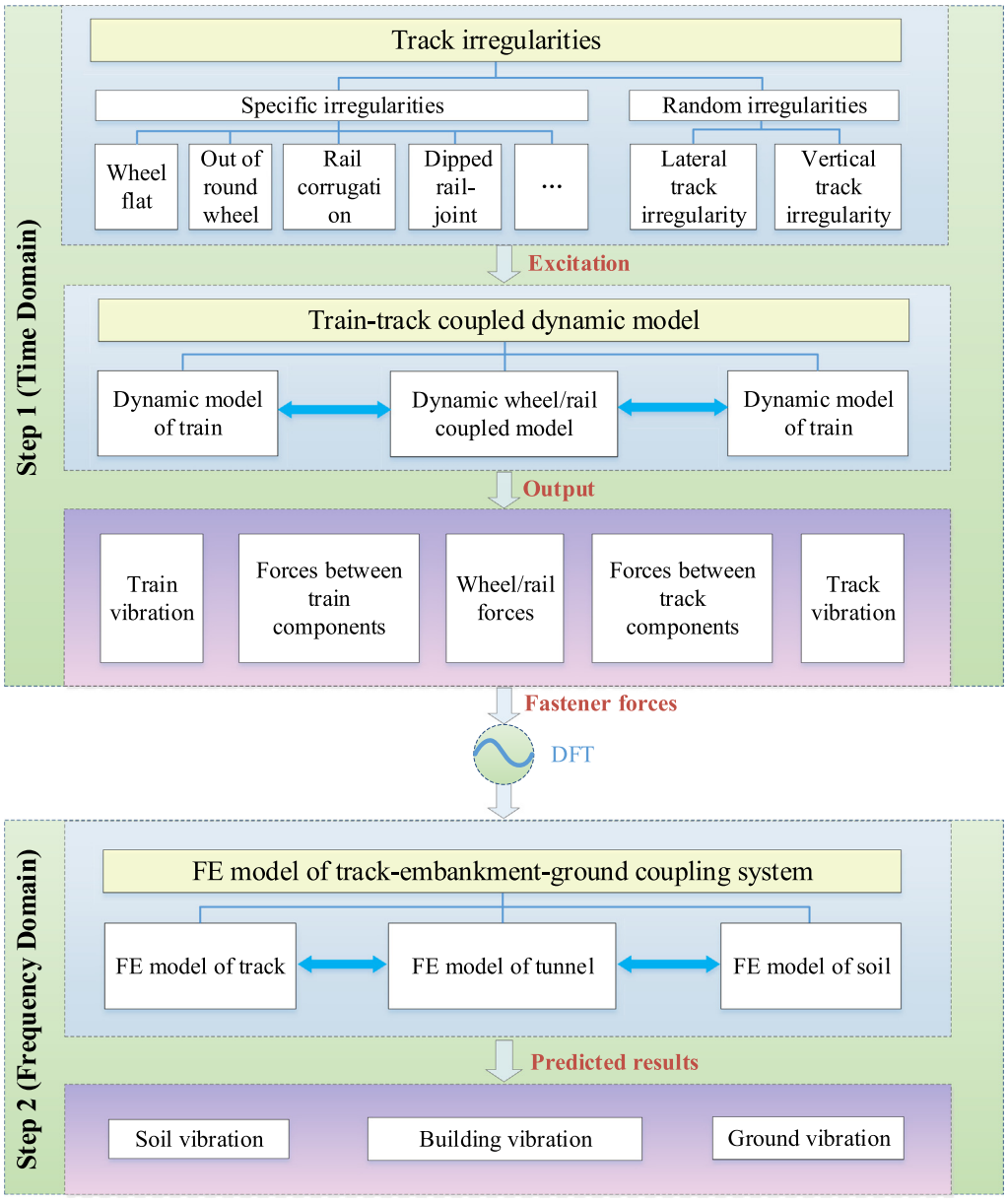

Fig. 3. Framework of numerical prediction methodology.

motion ϕ_r, each slab a vertical motion Z_s, a lateral motion Y_s, and rotation in the horizontal plane ψ_s. Each rail is described by the simply supported beam due to its large ratio of length to cross-section. The equations of motion of the rail are then given in the form of the fourth-order partial differential equations in the time domain. For the vertical vibration, the slab can be treated as a thin elastic rectangular

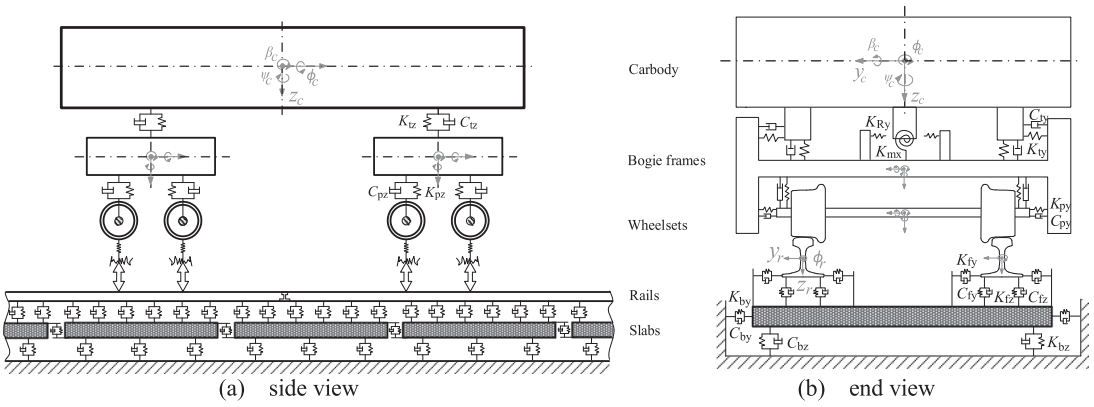

Fig. 4. Spatial vehicle-FST coupled dynamic model.

Table 1
DOFs of each vehicle.

Vehicle component	Lateral motion	Vertical motion	Roll motion	Yaw motion	pitch motion
Car body	Y_c	Z_c	ϕ_c	ψ_c	β_c
ith bogie frame ($i = 1, 2$)	Y_{ti}	Z_{ti}	ϕ_{ti}	ψ_{ti}	β_{ti}
jth wheelset ($j = 1$–4)	Y_{wj}	Z_{wj}	ϕ_{wj}	ψ_{wj}	β_{wj}

plate due to its large ratio of length and width to thick. Thus the vertical motion of the slab is also governed by the fourth-order partial differential equations in the time domain. For the lateral vibration and rotation in the horizontal plane, the slab can be regarded as the rigid body whose kinetic equation is second-order ordinary differential equation.

In order to lessen the difficulty of the solution procedure, all partial differential equations of the rails and slabs are transformed into a series of second-order ordinary differential equations by means of Ritz's method, and then a time-stepping integration method is adopted. The transformation results could be found in references (Zhai et al., 1996; Zhai et al., 2009; Zhai et al., 2013). The final equations of the FST could also be assembled into the standard matrix form, similar to Eq. (1), as

$$\mathbf{M}_T\ddot{\mathbf{Z}}_T + \mathbf{C}_T\dot{\mathbf{Z}}_T + \mathbf{K}_T\mathbf{Z}_T = \mathbf{F}_T\left(\mathbf{Z}_V, \dot{\mathbf{Z}}_V, \mathbf{Z}_T, \dot{\mathbf{Z}}_T\right) \tag{2}$$

in which $\mathbf{M}_T$, $\mathbf{C}_T$ and $\mathbf{K}_T$ are the mass, damping and stiffness matrices of the FST subsystem. $\mathbf{F}_T$ is the load vector involving the lateral and vertical wheel/rail forces.

It can be seen from Eqs. (1) and (2) that the wheel/rail forces are the key for solving the dynamic responses of the train-FST coupled system. The wheel/rail interaction is descripted by a dynamic wheel/rail coupling model developed by Chen and Zhai (2004), which takes into account three kinds of rail motions along the vertical, lateral and torsional directions.

In the train-FST coupled dynamic model, there are many nonlinear elements, such as the suspension forces and the wheel/rail forces, which are determined by the displacements and velocities the train-FST coupled system. Besides, the total number of the DOFs of the train-FST coupled system becomes large. To efficiently solve the nonlinear coupled dynamic system, the simple fast explicit integration method developed by Zhai (1996) is prefered.

2.2. FE model of track-tunnel-soil-building coupled dynamic system

The geometric construction of the building is so complex that only the FEM is competent to establish the dynamic model of the building. Considering the calculation efficiency and calculation accuracy, five types of elements are adopted to model the track-tunnel-soil-building coupled dynamic system in the general finite element software ANSYS. The slabs, the tunnel and the walls of the building are modelled by the 4-node shell elements SHELL63. The pillars of the building are respectively modelled by the BEAM188 elements. The layered soil is modelled by three dimensional solid elements SOIL45. The contact elements CONTA175 and TARGE170 are used to couple the node displacements between the shell elements and the soil elements at the interfaces, so that the relative displacements between the tunnel and the soil and between the soil and the building at the interfaces are zero. The FE model of track-tunnel-soil-building coupling dynamic system is illustrated in Fig. 5.

In reality, the soil is an infinite half-space. However, the volume of the soil has to be limited in the FE model and the wave will be therefore reflected at the boundary. In order to mitigate the boundary effect, artificial boundaries are adopted to encase the FE model. Artificial boundaries in the FE model can be easily implemented by modifying the material properties and fixing the outside nodes of the outermost elements (illustrated in Fig. 6). These boundaries and the modified outermost elements are referred to as consistent viscous-spring artificial boundaries and viscous-spring boundary elements (Gu et al., 2007). The material properties of the viscous-spring boundary elements are as follows:

- equivalent Poisson's ratio:

$$\nu' = \begin{cases} \dfrac{\alpha-2}{2(\alpha-1)}, & \alpha \geq 2 \\ 0, & \text{other} \end{cases} \tag{3}$$

- equivalent Young's modulus:

$$\mathrm{E}' = 2\alpha_T h \frac{G}{R}(1+\nu') \tag{4}$$

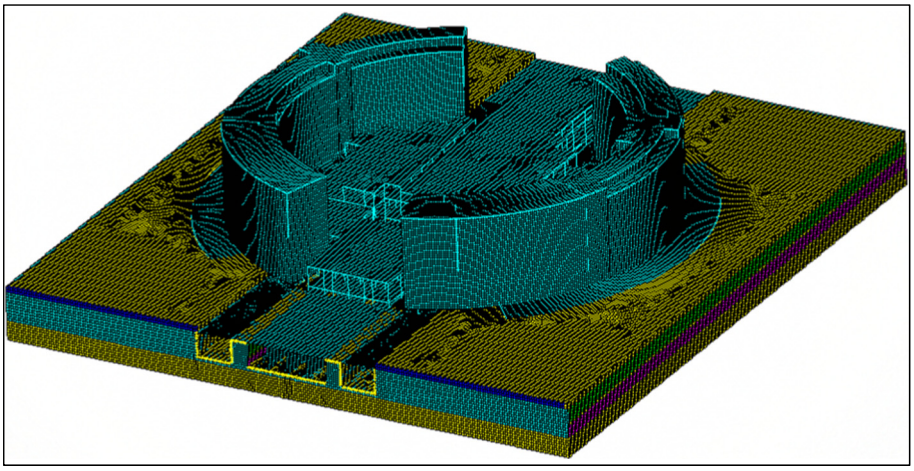

Fig. 5. FE model of track-tunnel-soil-building coupled dynamic system.

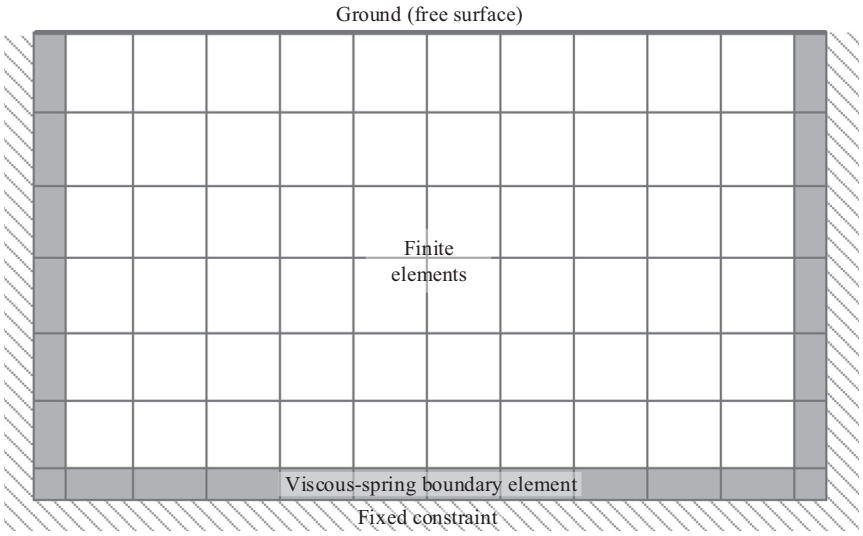

Fig. 6. Consistent viscous-spring artificial boundaries.

• equivalent damping ratio:

$$\eta' = \frac{\rho R}{3G}\left(2\frac{v_s}{\alpha_T} + \frac{v_p}{\alpha_N}\right) \quad (5)$$

where, $\alpha = \alpha_N/\alpha_T$, α_N and α_T are the parameters of the consistent viscous-spring artificial boundaries and are generally equal to 4.0 and 2.0, respectively; ρ and G are the density and shear modulus of the soil; h and R are the thickness of the viscous-spring boundary element and the distance between the source of scattering wave and the consistent viscous-spring artificial boundary; v_p and v_s are the velocities of pressure wave and shear wave of the soil, respectively.

3. Evaluation standards

In China, there are two relevant standards to evaluate and control the building vibration induced by the metro train. One is the national standard (China standard, 1988), *Standard of environmental vibration in urban area* (GB 10070-88), and the other one belongs to the industry standard (China industry standard, 2009), *Standard for limit and measuring method of building vibration and secondary noise caused by urban rail transit* (JGJ/T170-2009). The standard (GB 10070-88) adopts the frequency-weighted method, as stipulated in the international standard (ISO2631-1-1997), to calculate the weighted RMS acceleration as the vertical acceleration level (*VAL*) and regulates six types of limits and defines their application scope, listed in Table 2. The industry standard (JGJ/T170-2009) calculates the weighted one-third octave band RMS values of the vertical accelerations of the center frequencies 4–200 Hz, using a similar method with the international standard, as the vertical acceleration levels at individual frequencies (*VALIF*s). According to the standard (JGJ/T170-2009), buildings along the urban rail transit can be divided into 5 classes in terms of their functionality and the maximum of all *VALIF*s must be lower than the limits. The functional areas and the corresponding limits defined by the standard JGJ/T170-2009 are listed in Table 3, and the frequency weightings in one-third octaves are listed in Table 4.

In both standards, only the vertical acceleration is considered. Therefore, only the vertical vibration accelerations of the response points are calculated in this paper. In terms of the function of the hotel and referring the standard GB 10070-88, the hotel belongs to the residential area, whose *VAL* has to be below 70 dB in day-time and 67 dB in night-time. According to the standard JGJ/T170-2009, the hotel belongs to the Class 1, whose maximum of all *VALIF*s has to be below 65 dB in day-time and 62 dB in night-time.

Table 2
Classification and limits specified by standard (GB 10070-88).

Application scope	Limits (dB)	
	For night-time	For day-time
Special residential areas	65	65
Residential and cultural educational areas	67	70
Residential-commercial mixed areas, central business district	72	75
Industrial concentration district	72	75
Sides area of arterial road	72	75
Sides area of trunk railway	80	80

4. Prediction results

4.1. Dynamic parameters

The inertial characteristics, suspension parameters and characteristic lengths of the trains are the key parameters for modelling the effect

Table 3
Classification and limits specified by standard (JGJ/T170-2009).

Classes	Functional area	Limits (dB)	
		For night-time	For day-time
0	Special residential areas	62	65
1	Residential and cultural educational areas	62	65
2	Residential-commercial mixed areas, central business district	67	70
3	Industrial concentration district	72	75
4	Sides area of transportation main lines	72	75

Table 4
Frequency weightings in one-third octaves in JGJ/T 170-2009.

Frequencies (Hz)	4	5	6.3	8	10	12.5	16	20	25
Factors (dB)	0	0	0	0	0	-1	−2	−4	−6
Frequencies (Hz)	31.5	40	50	63	80	100	125	160	200
Factors (dB)	−8	−10	−12	−14	−17	−21	−25	−30	−36

Table 5
Main parameters of the metro train.

Vehicle	M_c (t)	M_t (t)	M_w (t)	J_c (t·m^2)	J_t (t·m^2)	K_p (MN/m)	C_p (kNs/m)	K_s (MN/m)	C_s (kNs/m)
Motor	49.08	4.42	1.68	1698.4	4.9	1.27	26	0.27	16.2
Trailer	52.22	2.39	1.4	1625.4	3.45	1.27	26	0.27	16.2

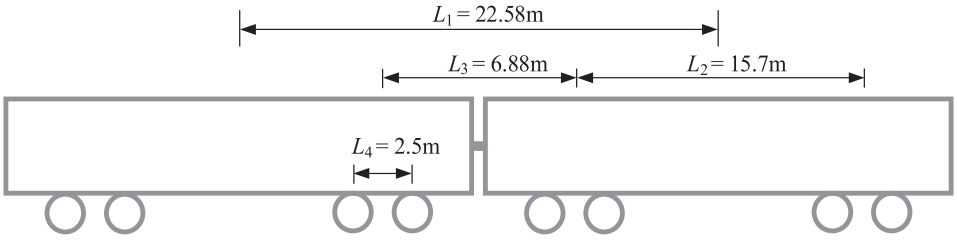

Fig. 7. Schematic main dimensions of the train.

of train on the dynamic responses of the track-tunnel-soil-building system (Zhai et al., 2015), which are shown in Table 5 and Fig. 7. In Table 5, M_c, M_t and M_w denote the mass of car body, bogie frame and wheelset, respectively; J_c and J_t are the moment of inertia of car body and bogie; K_p and C_p are the stiffness and damping of the primary suspension of the train (per axle box); K_s and C_s are the stiffness and damping coefficients of the secondary suspension (per bogie). The metro train is composed of 6 trailer vehicles and 2 motor vehicles as the head car and the tail car. The axle load of the full-loaded train is about 16 t.

There are two metro lines, i.e. four track lines, passing under the building. In order to isolate the vibration propagating from the track to the track base, all track lines are laid on the modified FST, which mainly consists of 60 kg/m rails, fastener systems, floating slabs and steel springs. The dynamic characteristics of the FST structure are given in Table 6. The concrete strength grade of the tunnel and the hotel is C35. The dynamic properties of the in-situ soil layers are shown in Table 7. The Young's modulus and damping ratio of the soil at the shear strain level of 10^{-5} are also presented.

The maximal operating speed of the two metro lines is 140 km/h. A metro station will be built beneath and near the hotel. In the operational planning, some trains will slow down entering the station and their speeds are about 80 km/h. However, in order to reach the airport with less time-consuming trips, some trains will pass through the station without stop and their speeds may reach up to the maximal operating speed.

4.2. Train-FST coupled dynamic responses

In the first step of the two-step numerical prediction method, the dynamic responses of the train-FST coupled system in time-domain will be presented when the dynamic parameters of the train and the track are used for the established train-track coupled dynamic model. The corresponding results in frequency-domain can be obtained using DFT. Some typical dynamic responses of the train-FST coupled system with the train speed of 80 km/h and 140 km/h are shown in Fig. 8.

When the train speed is 80 km/h, the maximal and mean values of the vertical wheel/rail force in time domain are 120.19kN and 79.26kN. As the train speed reaches 140 km/h, the time-domain maximum became larger and reaches up to 152.75kN. However, the mean value is 79.25kN which almost not changes, because it is mainly induced by the axle load. In the frequency domain, the maximal amplitudes of the vertical wheel/rail forces are 1.35kN and 2.45kN, respectively corresponding to the train speeds 80 km/h and 140 km/h, around the frequency of 45 Hz, which may be caused by the wheel/rail resonance. Higher train speed leads to greater wheel/rail forces and severer interaction between train and the track which will aggravate the vibration of the track. For example, with the train speed increasing from 80 km/h to 140 km/h, the time-domain maximum of the vertical acceleration of the slab at the central position increases from 1. 29 g to 2 .5g.

The vertical and lateral fastener forces are illustrated in Fig. 8(b) and (c). When the train speed is 80 km/h, the time-domain maxima of the vertical and lateral fastener forces are 33.68kN and 1.96kN. As the train speed increases to 140 km/h, the time-domain maxima of the vertical and lateral fastener forces are respectively increased to 38.27kN and 2.86kN. In the frequency domain, the fastener force amplitude has some significant frequency components in the spectra. The significant frequencies are found to be close to the integral multiple of the characteristic frequencies, $f_i = v/L_i$, induced by the vehicle speed v and train characteristic length L_i (see Fig. 7). It is found that higher train speed leads to more drastic fastener forces. Therefore, it could be draw out that the train moving on the track with higher speed would bring out severer building vibration.

4.3. Building vibration induced by moving train

The fastener forces, obtained in the first step of the two-step numerical prediction method, are taken as the external loads of the FE model of track-tunnel-soil-building coupling system to solve the building vibration induced by the train passing beneath the building. A specific

Table 6
Dynamic parameters of FST.

Component	Parameters	Values
Slab	Length × width × thickness (m)	24.97 × 4.2 × 0.42
	Density (t/m^3)	2.5
	Young's modulus (GPa)	35
	Poisson's ratio	0.25
Fasteners	Vertical stiffness (MN/m)	30
	Lateral stiffness (MN/m)	15
	Damping ratio	0.2
Steel springs	Vertical stiffness (MN/m)	6.6
	Lateral stiffness (MN/m)	15
	Damping ratio	0.1

Table 7
Dynamic properties of soil.

Layer	Thickness (m)	Density (t/m^3)	Young's modulus (MPa)	Poisson's ratio	Damping ratio
(1)	2.0	1.75	85	0.404	0.05
(2)	7.5	2.0	96	0.395	0.05
(3)	3.8	2.15	1271	0.311	0.05
(4)	48.4	2.5	5096	0.295	0.05

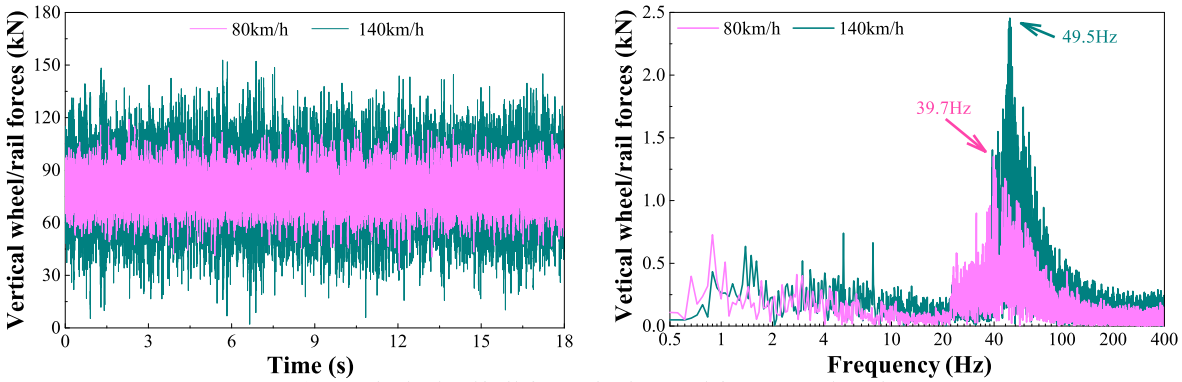

(a) Vertical wheel/rail forces in time and frequency domain

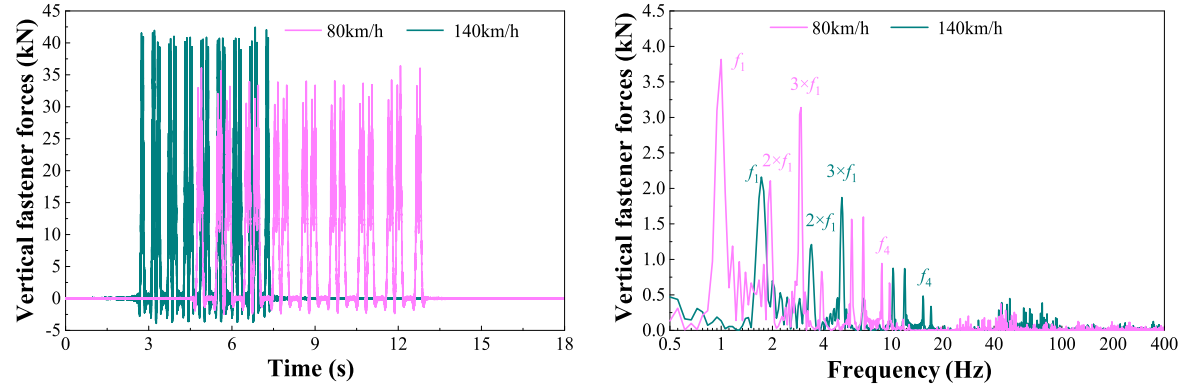

(b) Vertical fastener forces in time and frequency domain

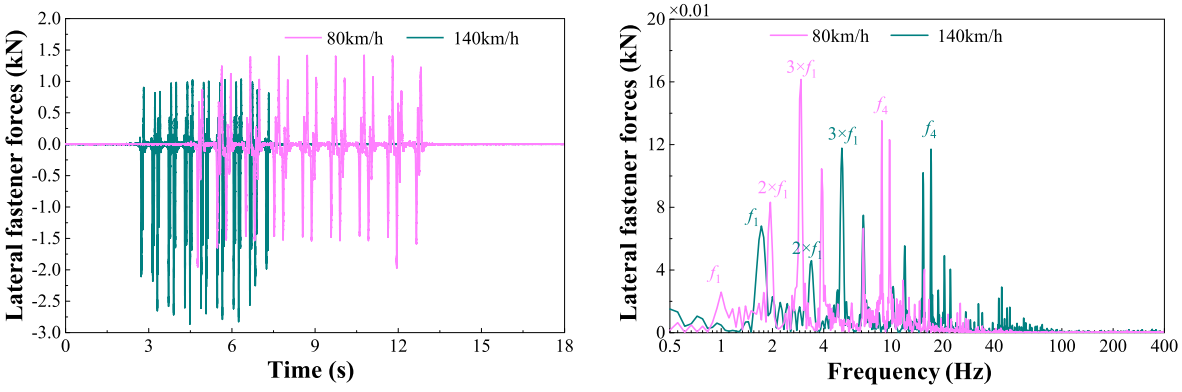

(c) Lateral fastener forces in time and frequency domain

Fig. 8. Dynamic responses of train-FST coupled system in time-domain and frequency-domain for different train speeds.

attention was paid to the vibration evaluation of the main building which is used for accommodation. Therefore, the vibration of the floor at the central point of the room in the main building is taken as an evaluation index. Additionally, the two parts of the main building are almost symmetrical (see Fig. 9). Thus, only one part of the main building is taken into consideration. Finally, 52 response points L1~L52 (shown in Fig. 9) on each floor of the main building are taken into consideration. In Fig. 7, the green arrows present the directions of the train running on both metro lines. In this section, the building vibrations are acquired in the case of a single train running with the speed of 80 km/h and 140 km/h in the direction 1 (see Fig. 9), and the reducing vibration measure is not used.

Fig. 10 shows the *VALIF*s of some response points, including the 62 dB limit for night-time (blank line) and 65 dB limit for day-time (gray line) defined by the standard JGJ/T170-2009. Similar *VALIF*s are obtained for other response points and thus are not given in this paper.

The train running with a speed of 80 km/h has given rise to the maxima of *VALIF*s of some response points exceeding the limits, and the maxima of *VALIF*s of all response points are concentrated in the frequency range of 20–50 Hz. With the train speed increasing to 140 km/h, *VALIF*s of more response points exceed the limit, and the frequency distribution range of the maximums of *VALIF*s is extended to 20–80 Hz. For each response point, the greater train speed leads to the greater *VALIF*s at most frequencies, indicating that the train running with a higher speed will result in more serious building vibration. With the frequency increasing, the increment of the *VALIF*s caused by the train speed increasing is more obvious, which might be due to the greater amplitudes of the fastener forces induced by the train running with higher speeds (see Fig. 8). Whether the train speed is 80 km/h or 140 km/h, the variations of the *VALIF*s of all response points have a similar tendency that the *VALIF*s increase at first and then decrease as the frequencies increase.

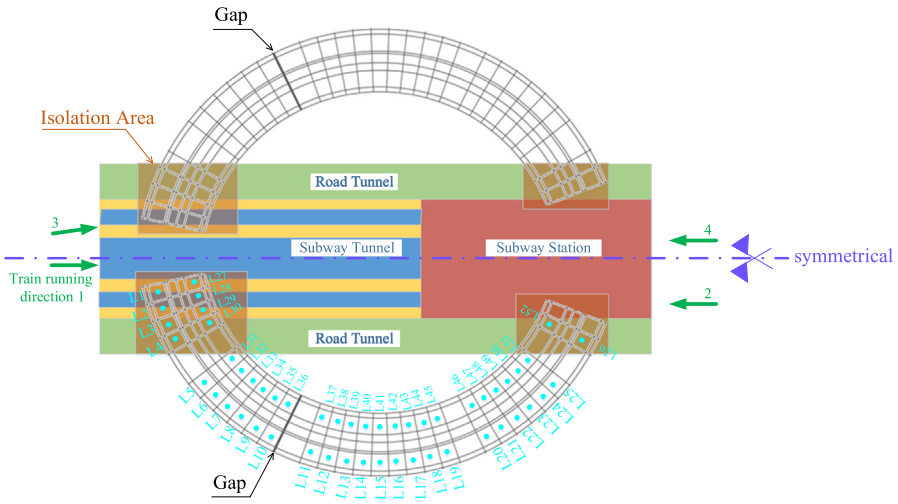

Fig. 9. Birdseye view of the tunnel, the rooms in the main building and the response points.

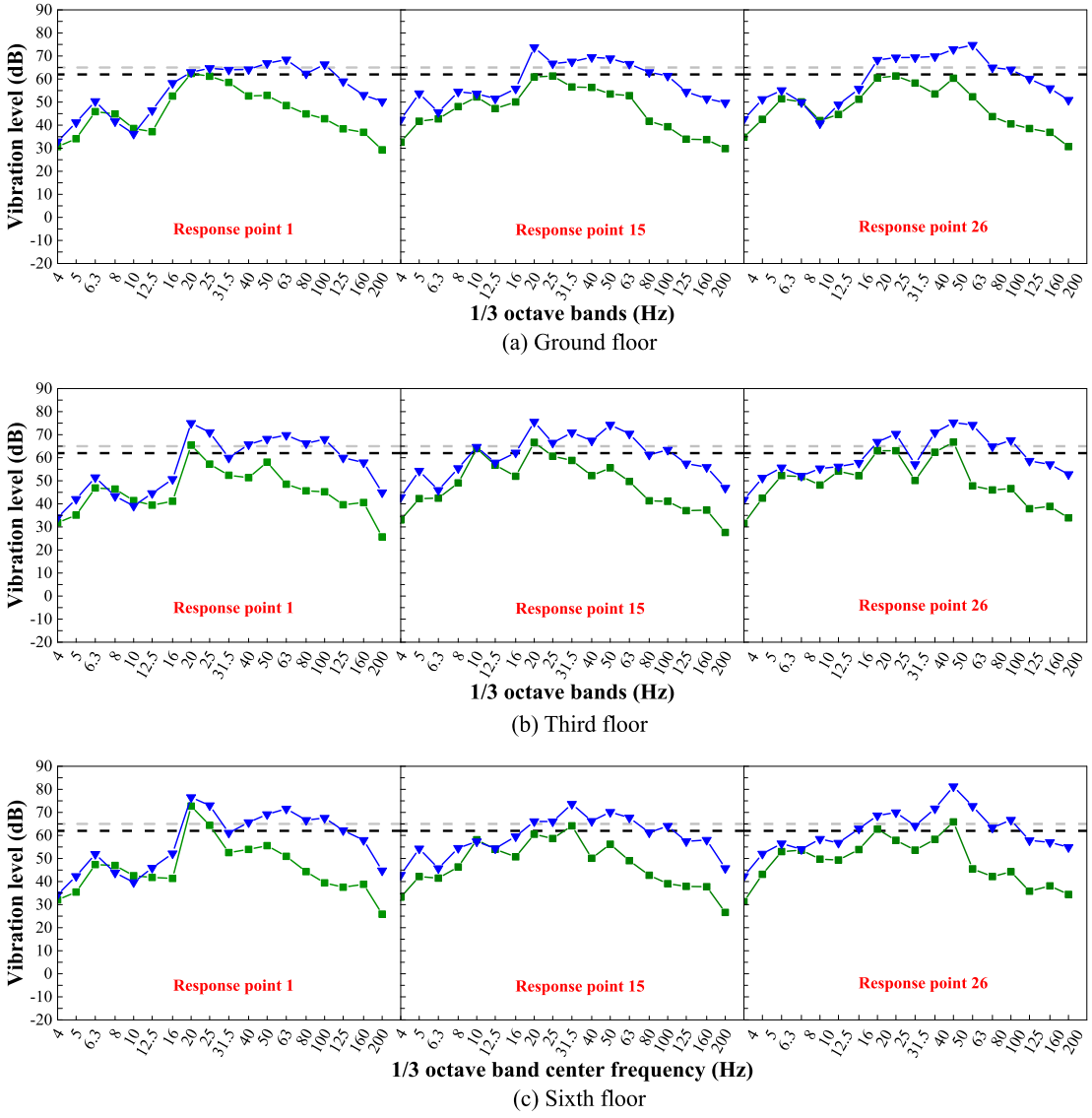

Fig. 10. *VALIFs* of some response points. —■— and —▼— represent the train speeds of 80 km/h and 140 km/h, respectively. The blank and gray dashed lines represent the limits defined by the standard JGJT170-2009.

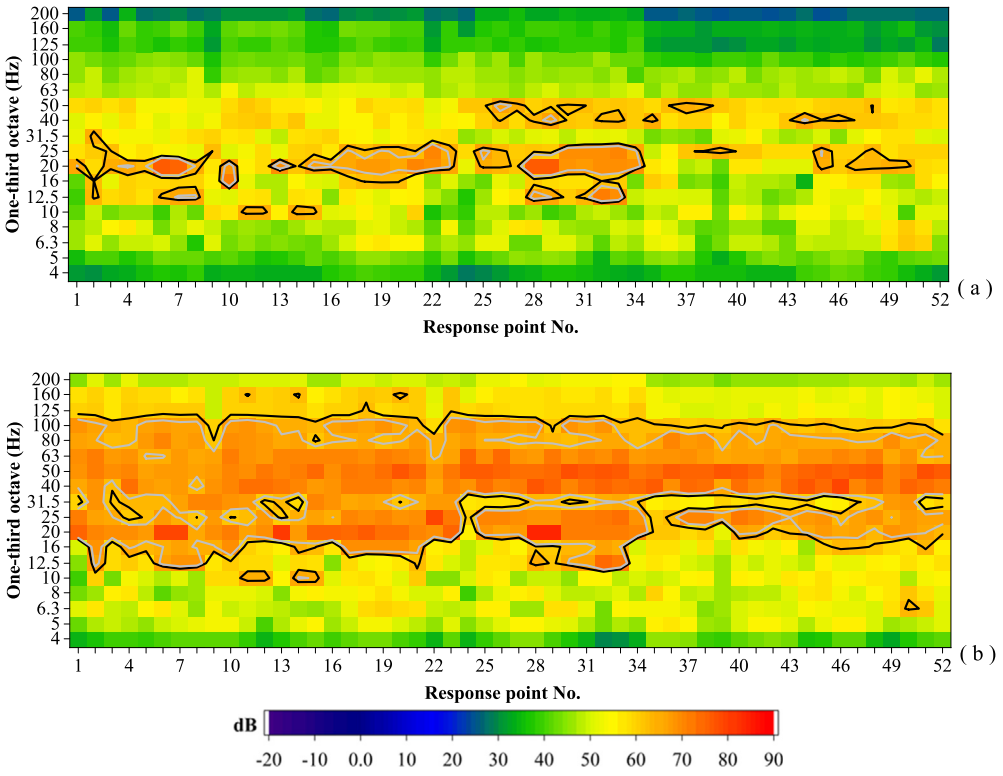

Fig. 11. *VALIF*s of the response points on the third floor, induced by the train running with the speed of: (a) 80 km/h and (b) 140 km/h. Black and gray lines represent the limits specified by standard JGJ/T170-2009.

In order to clearly reveal the frequency distribution of the *VALIF*s of all response points, the *VALIF*s of all response points on the third floor induced by the train running with the speed of 80 km/h and 140 km/h are illustrated in Fig. 11. The *VALIF*s of response points on other floors have the similar distribution. It can be clearly found that the *VALIF*s out of the limits are in the frequency range of 10–50 Hz in the case of train speed of 80 km/h, however, when the train speed is 140 km/h, the frequency range of the *VALIF*s out of the limits is enlarged, whose lower boundary is 6 .3Hz and upper boundary reaches up to 160 Hz. Fig. 11 also illustrates that the higher train speed results in more *VALIF*s of each response points and more response points exceeding the limits. In the case of train speed of 80 km/h, the vibrations of some response points on the third floor do not exceed the limit for night-time, however, as the train speed increases to 140 km/h, the vibrations of all response points on the third floor exceed the limit for day-time.

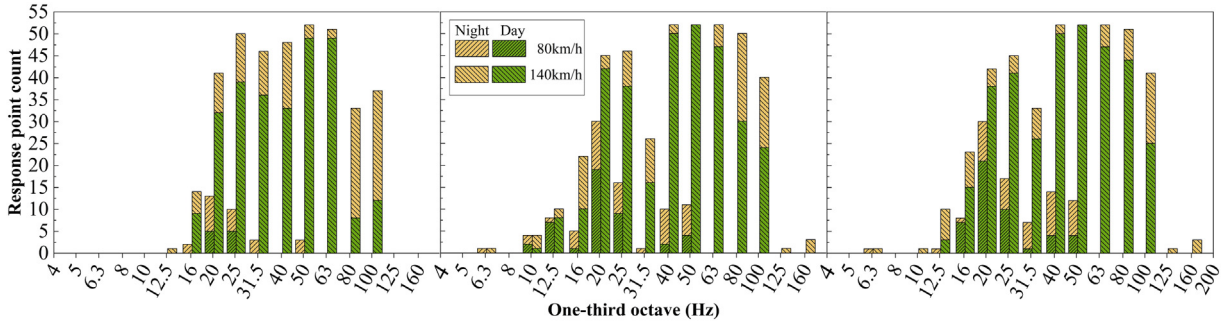

Fig. 12. Number of response points exceeding limits specified by standard JGJ/T170-2009, left: ground floor, middle: third floor, right: sixth floor.

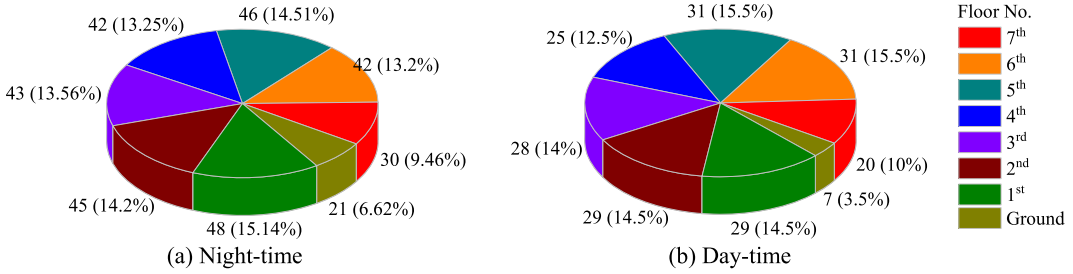

Fig. 13. Number of response points exceeding limits specified by standard JGJ/T170-2009. Train speed is 80 km/h.

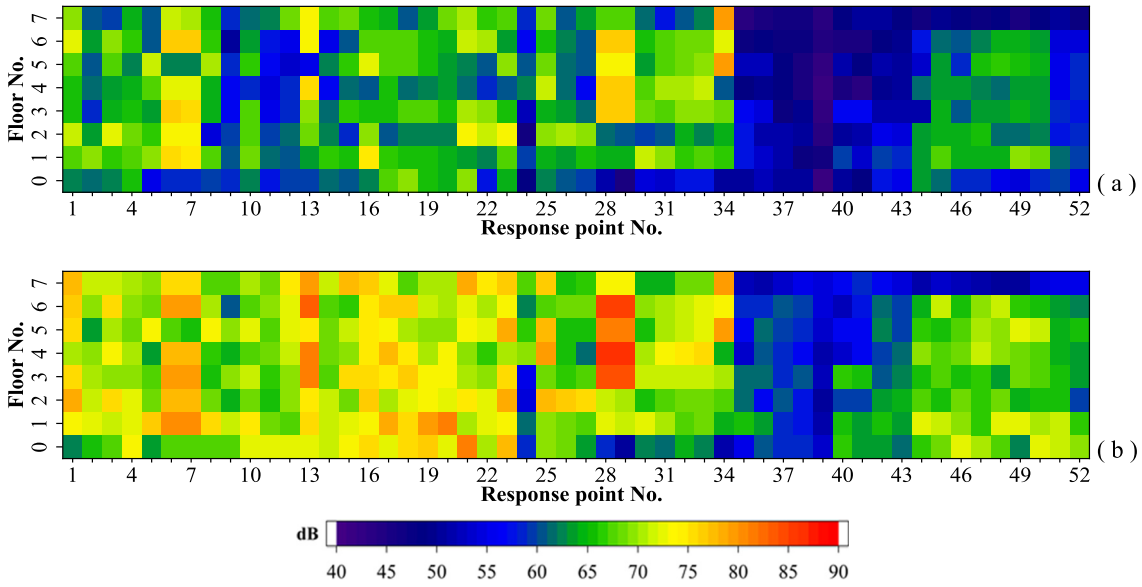

Fig. 14. *VALIF*s of all response points at the center frequency of 20 Hz, induced by the train running with the speed of: (a) 80 km/h and (b) 140 km/h.

The number of the over-limit response points at every octave band is listed in Fig. 12. Other floors have a similar statistical result shown as Fig. 12. In the case of a train speed of 80 km/h and for all floors, the frequency 20 Hz is the most favorite central frequency for which the number of the over-limit response points is the most critical. Nevertheless, the ratio of the response points exceeding the limits is only about 60% at the central frequency 20 Hz. Fig. 12 also shows that the *VALIF*s out of the limits are in the frequency range of 10–50 Hz in the case of train speed of 80 km/h; however, when the train speed reaches 140 km/h, the frequency range of the *VALIF*s out of the limits are enlarged, whose lower boundary is 6 .3 Hz and upper boundary reaches up to 160 Hz. Additionally, the higher train speed brings out more response points exceeding the limits at every frequency. Especially in the frequency range of 40–80 Hz, almost all of response points exceeding the limits. The higher train speed also leads the larger ratio of the response points exceeding the limit for day-time.

Fig. 13 summarizes the numbers of the over-limit response points on each floor and their ratios to the total number of the over-limit response points on all floors. Only the results of the train speed of 80 km/h are given here, because when the train speed is 140 km/h, almost all of the response points on each floor exceed the limits for both night-time and day-time as shown in Fig. 11(b). It can be found from Fig. 13 that the first floor contributes the most over-limit response points in terms of the limit for night-time, however, in terms of the response

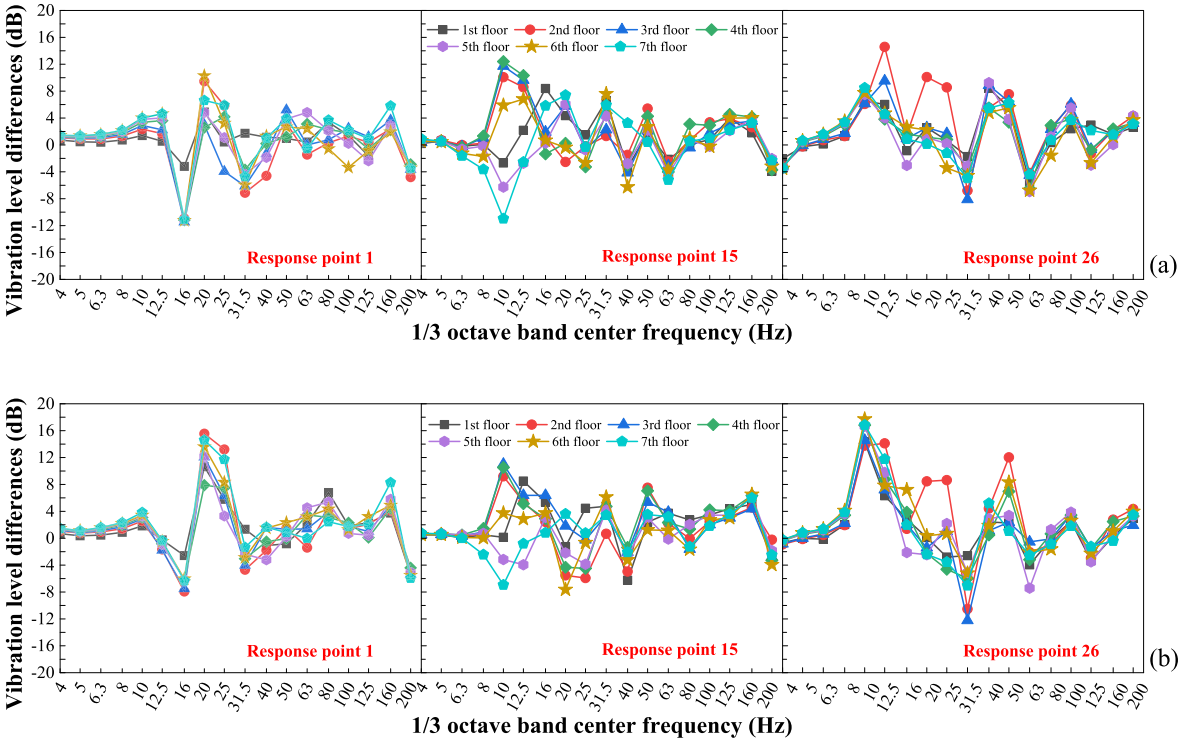

Fig. 15. *VALIF* amplification factors relative to ground floor, with the train speed of: (a) 80 km/h and (b) 140 km/h.

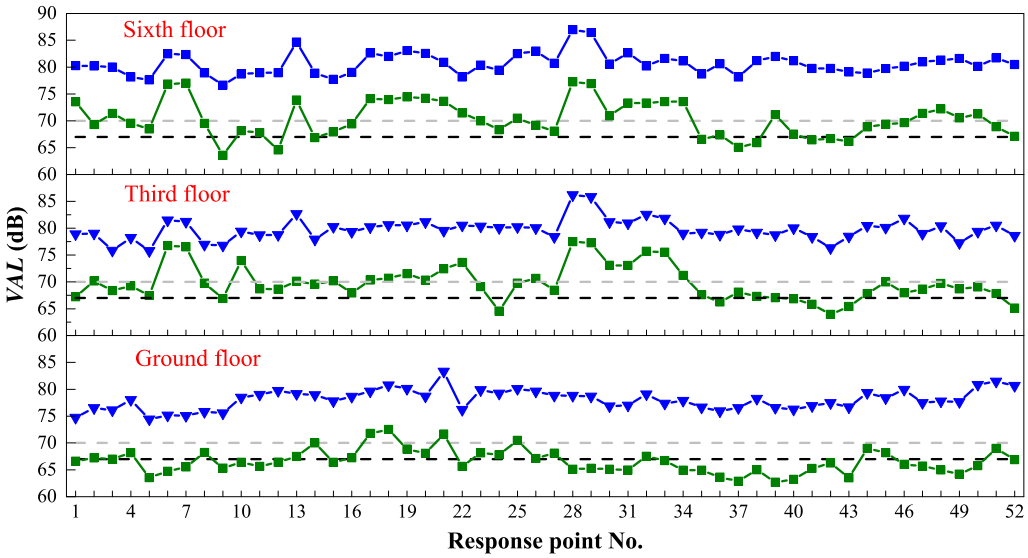

Fig. 16. *VAL*s of some response points. —■— and —▼— represent the train speeds of 80 km/h and 140 km/h, respectively. The blank and gray lines represent the limits defined by the standard GB 10070-88.

points exceeding the limit for day-time, the contributions of the fifth and sixth floors are the same and larger than other floors.

The variation of the *VALIF*s with the story height is irregular, as shown in Fig. 14. This phenomenon also appears at other central frequencies, so they are not shown here. Nevertheless, some regularity could be found in the vibration amplification relative to the ground floor, instanced by the *VALIF* amplification factors as shown in Fig. 15. There are notable vibration amplifications from the ground floor to the upper floors due to structural resonances. The same phenomenon can be also found in the measured structural vibration induced by the adjacent subway networks (Vogiatzis and Mouzakis, 2018). Here the maximal increases are approximately equal to 14 dB and 18 dB, respectively for the train speed 80 km/h and 140 km/h.

Fig. 16 collects the frequency-weighted *VAL*s of some response points, using the method stipulated in the international standard ISO2631-1-1997. In the graphs, the blank and gray lines represent the limits 67 dB for night-time and 70 dB for day-time defined by the standard GB 10070-88, respectively. It is found that, when the train speed is 80 km/h, the *VAL*s of some response points are below the limit for night-time regulated by the standard GB 10070-88 and the ratio of the response points exceeding the limit for day-time is very small. However, as the train speed is 140 km/h, the *VAL*s of all response points are greater than the limit for day-time. Compared to the train speed of 80 km/h, The *VAL*s of all response points are increased about 10 dB as the train speed increases from 80 km/h to 140 km/h.

5. Vibration reduction analysis

The results in Section 4 show that in spite of the FST owning excellent vibration isolation performance, the building vibrations exceed the limits specified by the standards GB 10070-88 and JGJ/T170-2009, no matter the single train runs at the speed of 80 km/h or 140 km/h. This will seriously affect the comfort of the hotel, and even brings adverse impact on the sleep qualities of the residents during night. Hence, some reducing vibration measures have to be used. Although the additional vibration reduction measures implemented on the track can further reduce the vibration propagation and noise radiation from the track to the building (Vogiatzis and Vanhonacker, 2016; Zhu et al., 2017), the widely used base isolation techniques (Masoud et al., 2013; Ulgen et al., 2016) may have better performance on isolating the vibration propagation to the building in a wide frequency range. The architectural designers of the hotel are planning to adopt a base isolation measure, namely the structural vibration of the building is reduced by installing steel springs between the superstructure and the base, as shown in Fig. 17. The pillars of the building constructed on the tunnel

(a) steel spring (b) install location

Fig. 17. Steel spring of base isolation.

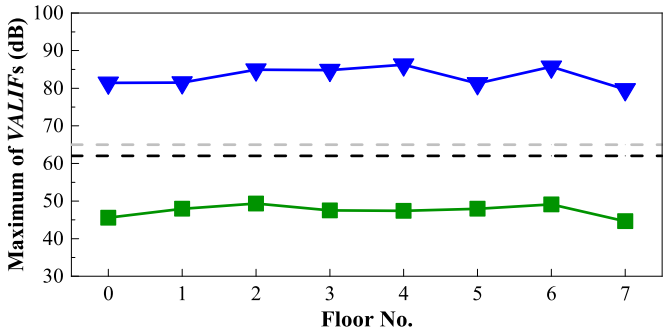

Fig. 18. Maxima of *VALIF*s of all response points on each floor with isolation (—■—) and no isolation (—▼—). The blank and gray lines represent the limits defined by the standard JGJ/T170-2009.

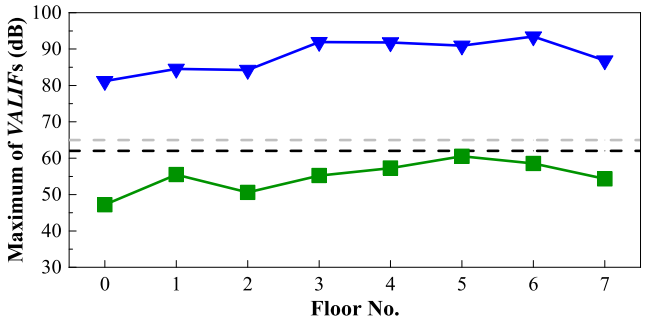

Fig. 20. Maxima of *VALIF*s of all response points on each floor with isolation (—■—) and no isolation (—▼—). The blank and gray dashed lines represent the limits defined by the standard JGJ/T170-2009.

are truncated by steel springs, as shown in Fig. 17(b). The area of the install locations is illustrated in Fig. 9.

Whether the train speed is 80 km/h or 140 km/h, the variations of the *VALIF*s of all response points have a similar tendency. Besides, the greater train speed leads to greater *VALIF*s at most frequencies. So the vibration reduction performance of the base isolation measure is implemented with the train speed of 140 km/h.

Fig. 18 shows the influence of base isolation on the maximum of the *VALIF*s of all response points on each floor. It can be found that before the base isolation was adopted, the maximums of the *VALIF*s of every floor are much larger than the limit for day-time regulated by the standard JGJ/T170-2009. With the base isolation being installed, the maximums of the *VALIF*s of every floor are reduced by about 30 dB and are below the limit for night-time. Thus, the base isolation can bring about building vibration satisfying the standard JGJ/T170-2009.

The base isolation also forces the building vibration to satisfy the standard GB 10070-88. In order to illustrate this, a figure similar to Fig. 16 is given in Fig. 19. Without the base isolation, the *VAL*s of all response points are higher than the limit for day-time specified by the standard GB 10070-88. The base isolation decreases the *VAL*s of all response points by about 30dB, so all response points satisfy the standard GB 10070-88.

The above studies are implemented in the case of a single train running along the direction 1 in Fig. 9. In order to further explore whether the base isolation can guarantee the building vibration to meet the requirements of the standards in the worst conditions, the vibration reduction performance of the base isolation measure is implemented in the extreme case that four trains are simultaneously running with the speed of 140 km/h along the directions 1–4 of both metro lines. In this case, the *VALIF*s of the response points are indeed increased, especially its maximum that overshoots 90 dB, as shown in Fig. 20. Without the base isolation, the maximum of *VALIF*s of each response point is overlimit. The base isolation distinctly attenuates the *VALIF*s of each response point so that the vibrations of all response points satisfy the standard JGJ/T170-2009. The *VAL*s of the response points also increase in the extreme case, comparing the Fig. 21 with Fig. 19. Without the base isolation, the *VAL*s of all response points are higher than the limit for day-time specified by the standard GB 10070-88. The base isolation decreases the *VAL*s of all response points by about 30dB, so all response points satisfy the standard GB 10070-88.

6. Conclusions

A two-step prediction method for the building vibration induced by moving train has been proposed in this work. In the first step, the

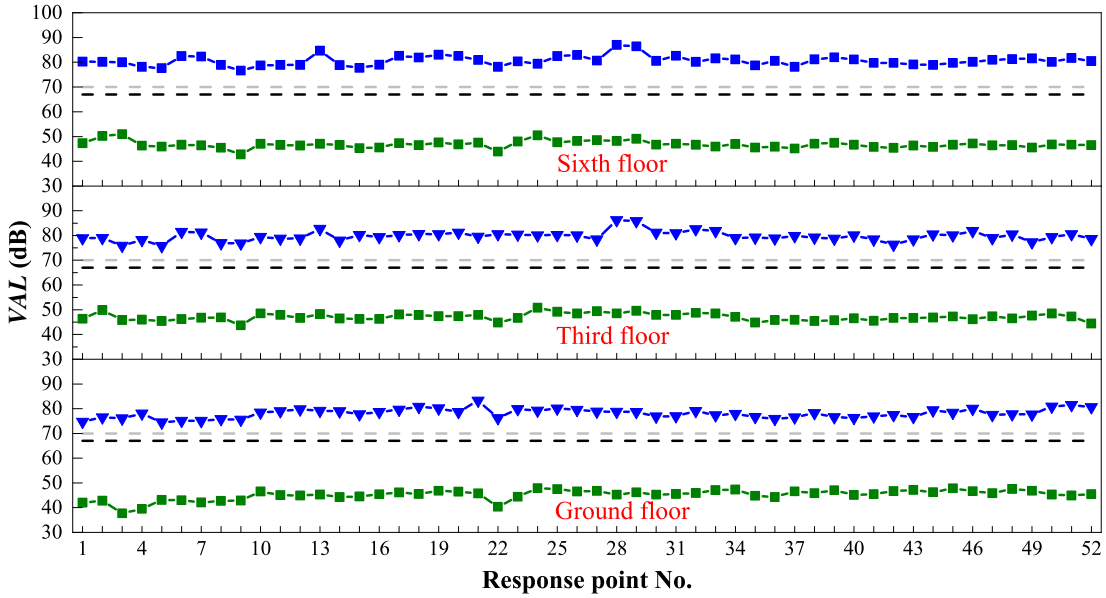

Fig. 19. *VAL*s of some response points with isolation (—■—) and no isolation (—▼—). The blank and gray dashed lines represent the limits defined by the standard GB 10070-88.

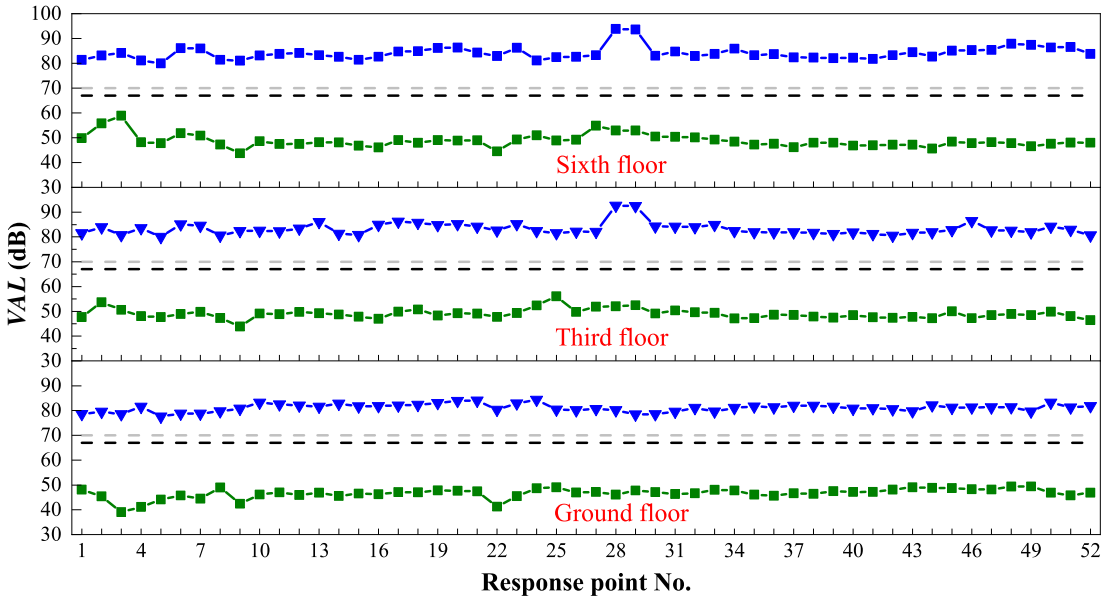

Fig. 21. *VALs* of some response points with isolation (—■—) and no isolation (—▼—). The blank and gray dashed lines represent the limits defined by the standard GB 10070-88.

dynamic responses of the train-track coupled system have been computed using a spatial train-track dynamic interaction model. Then the fastener forces have been taken as the external loads of a FE model of a track-tunnel-soil-building coupling system to obtain the building vibration at each floor. Vibrations of the large-scale building induced by underground train have been predicted under different train operation conditions, and a base isolation measure has been employed to control the over-limit building vibration. Main conclusions can be drawn as follows.

(1) The train running with the higher speed leads to the greater wheel/rail forces and aggravates the vibration of the track. The higher train speed also causes the severer building vibration and extends the frequency distribution range of the maximums of *VALIF*s.
(2) According to the relevant evaluation standards, prediction results have proven that the building vibration induced by underground train exceeds the standard limits.
(3) The base isolation measure can decrease the *VALs* of all response points of the building by about 30 dB. Even under extreme operation conditions, the structural vibration of the building with the base isolation can satisfy the relevant standard requirements.

Acknowledgement

This work was supported by the National Natural Science Foundation of China (No. 11790283, No. 51708457, No. 51868037), and the Introducing Talents of Discipline to Universities (111 Project) (Grant No. B16041). The authors would like to acknowledge the support from Sichuan Province Airport Group Co., Ltd.

References

Cai, C., He, Q., Zhu, S., et al., 2019. Dynamic interaction of suspension-type monorail vehicle and bridge: numerical simulation and experiment. Mech. Syst. Signal Process. 118, 388–407.
Chen, G., Zhai, W.M., 2004. A new wheel/rail spatially dynamic coupling model and its verification. Veh. Syst. Dyn. 41, 301–322.
China industry standard, 2009. JGJ/T 170-2009: Standard for Limit and Measuring Method of Building Vibration and Secondary Noise Caused by Urban Rail Transit (In Chinese).
China standard, 1988. GB 10070-88: Standard of Environmental Vibration in Urban Area (In Chinese).
Clouteau, D., Arnst, M., Al-Hussaini, T., et al., 2005. Free field vibrations due to dynamic loading on a tunnel embedded in a stratified medium. J. Sound Vib. 283, 173–199.
Connolly, D.P., Kouroussis, G., Woodward, P.K., et al., 2014. Scoping prediction of re-radiated ground-borne noise and vibration near high speed rail lines with variable soils. Soil Dyn. Earthq. Eng. 66, 78–88.
Connolly, D., Marecki, G.P., Kouroussis, G., et al., 2016. The growth of railway ground vibration problems - a review. Sci. Total Environ. 568, 1276–1282.
Coulier, P., Lombaert, G., Degrande, G., 2014. The influence of source-receiver interaction on the numerical prediction of railway induced vibrations. J. Sound Vib. 333, 2520–2538.
Degrande, G., Clouteau, D., Othman, R., et al., 2006. A numerical model for ground-borne vibrations from underground railway traffic based on a periodic finite element-boundary element formulation. J. Sound Vib. 293, 645–666.
Galvin, P., Romero, A., Domínguez, J., 2010. Fully three-dimensional analysis of high-speed train-track-soil-structure dynamic interaction. J. Sound Vib. 329, 5147–5163.
Gu, Y., Liu, J.B., Du, Y.X., 2007. 3D consistent viscous-spring artificial boundary and viscous-spring boundary element. Eng. Mech. 24, 31–37.
Gupta, S., Degrande, G., Lombaert, G., 2009. Experimental validation of a numerical model for subway induced vibrations. J. Sound Vib. 321, 786–812.
Han, H.Y., Zhai, W.M., 2011. Numerical simulation of soft ground vibration caused by high-speed trains. Advances in Environmental Vibration. Science Press, Beijing, pp. 142–150.
Hung, H., Yang, Y., 2010. Analysis of ground vibrations due to underground trains by 2.5D finite/infinite element approach. Earthq. Eng. Eng. Vib. 9, 327–335.
Hunt, H.E.M., 1996. Modelling of rail vehicles and track for calculation of ground vibration transmission into buildings. J. Sound Vib. 193, 185–194.
Hussein, M., Hunt, H., 2007. A numerical model for calculating vibration from a railway tunnel embedded in a full-space. J. Sound Vib. 305, 401–431.
International standard, 1997. ISO 2631-1-1997: Mechanical Vibration and Shock - Evaluation of Human Exposure to Whole-Body Vibration - Part 1: General Requirements.
Kouroussis, G., Verlinden, O., 2013. Prediction of railway induced ground vibration through multibody and finite element modelling. Mech. Sci. 4, 167–183.
Kouroussis, G., Verlinden, O., Conti, C., 2012. A two-step time simulation of ground vibrations induced by the railway traffic. Proc. Inst. Mech. Eng. C J. Mech. Eng. Sci. 226, 454–472.
Kouroussis, G., Connolly, D.P., Verlinden, O., 2014a. Railway-induced ground vibrations - a review of vehicle effects. Int. J. Rail Transp. 2, 69–110.
Kouroussis, G., Pauwels, N., Brux, P., et al., 2014b. A numerical analysis of the influence of train characteristics and rail profile on railway traffic ground-borne noise and vibration in the Brussels region. Sci. Total Environ. 482-483, 452–460.
Lombaert, G., Degrande, G., 2001. Experimental validation of a numerical prediction model for free field traffic induced vibrations by in situ experiments. Soil Dyn. Earthq. Eng. 21, 485–497.
Lopes, P., Costa, P.A., Calçada, R., et al., 2014a. Influence of soil stiffness on building vibrations due to railway traffic in tunnels: numerical study. Comput. Geotech. 61, 277–291.
Lopes, P., Costa, P.A., Ferraz, M., et al., 2014b. Numerical modeling of vibrations induced by railway traffic in tunnels: from the source to the nearby buildings. Soil Dyn. Earthq. Eng. 61-62, 269–285.
Lopes, P., Ruiz, J.F., Costa, P.A., et al., 2016. Vibrations inside buildings due to subway railway traffic. Experimental validation of a comprehensive prediction model. Sci. Total Environ. 568, 1333–1343.

Madshus, C., Bessason, B., Harvik, L., 1996. Prediction model for low frequency vibration from high speed railways on soft ground. J. Sound Vib. 193, 195–203.
Masoud, S., Anish, K.P., Moore, J.A., et al., 2013. Measurement of building foundation and ground-borne vibrations due to surface trains and subways. Eng. Struct. 53, 102–111.
Masoud, S., Anish, K.P., Moore, J.A., et al., 2014. Measurement and prediction of train-induced vibrations in a full-scale building. Eng. Struct. 2014 (77), 119–128.
Santos, N.C., Barbosa, J.M., Calcada, R., et al., 2017. Track-ground vibrations induced by railway traffic: experimental validation of a 3D numerical model. Soil Dyn. Earthq. Eng. 97, 324–344.
Shao, M.H., Zhai, W.M., Song, X.L., et al., 2013. Numerical simulation of high-speed train induced ground vibration for non-ballasted railway on embankment. 6th International Symposium on Environmental Vibration, Shanghai, November 8–10.
Sheng, X., Jones, C.J.C., Thompson, D.J., 2004. A theoretical model for ground vibration from trains generated by vertical track irregularities. J. Sound Vib. 272, 937–965.
Thompson, D., 2009. Railway Noise and Vibration. Mechanisms, Modelling and Means of Control. Elsevier Ltd, Oxford, UK.
Ulgen, D., Ertugrul, O.L., Ozkan, M.Y., et al., 2016. Measurement of ground borne vibrations for foundation design and vibration isolation of a high-precision instrument. Measurement 93, 385–396.
Verbraken, H., Lombaert, G., Degrande, G., 2011. Verification of an empirical prediction method for railway induced vibrations by means of numerical simulations. J. Sound Vib. 330, 1692–1703.
Vogiatzis, K., Kouroussis, G., 2015. Prediction and efficient control of vibration mitigation using floating slabs: practical application at Athens metro lines 2 and 3. Int. J. Rail Transp. 3, 215–232.
Vogiatzis, K., Mouzakis, H., 2018. Ground-borne noise and vibration transmitted from subway networks to multi-storey reinforced concrete buildings. Transp. 33, 446–453.
Vogiatzis, K., Vanhonacker, P., 2016. Noise reduction in urban LRT networks by combining track based solutions. Sci. Total Environ. 568, 1344–1354.
Vogiatzis, K., Zafiropoulou, V., Mouzakis, H., et al., 2018. Monitoring and assessing the effects from metro networks construction on the urban acoustic environment: the Athens metro line 3 extension. Sci. Total Environ. 639, 1360–1380.
Xia, H., Zhang, N., Cao, Y.M., et al., 2005. Experimental study of train-induced vibrations of environments and buildings. J. Sound Vib. 280, 1017–1029.
Xia, H., Chen, J., Wei, P., et al., 2009. Experimental investigation of railway train-induced vibrations of surrounding ground and a nearby multi-story building. Earthq. Eng. Eng. Vib. 8, 137–148.
Zhai, W.M., 1996. Two simple fast integration methods for large-scale dynamic problems in engineering. Int. J. Numer. Methods Eng. 39, 4199–4214.
Zhai, W.M., Cai, C.B., Guo, S.Z., 1996. Coupling model of vertical and lateral vehicle/track interactions. Veh. Syst. Dyn. 26, 61–79.
Zhai, W., Wang, K., Cai, C., et al., 2009. Fundamentals of vehicle-track coupled dynamics. Veh. Syst. Dyn. 47, 1349–1376.
Zhai, W., Xia, H., Cai, C., et al., 2013. High-speed train-track-bridge dynamic interactions – part I: theoretical model and numerical simulation. Int. J. Rail Transp. 1, 3–24.
Zhai, W., Wei, K., Song, X., et al., 2015. Experimental investigation into ground vibrations induced by very high speed trains on a non-ballasted track. Soil Dyn. Earthq. Eng. 72, 24–36.
Zhang, X., Zhai, W., Chen, Z., et al., 2018. Characteristic and mechanism of structural acoustic radiation for box girder bridge in urban rail transit. Sci. Total Environ. 627, 1303–1314.
Zhu, S., Wang, J., Cai, C., et al., 2017. Development of a vibration attenuation track at low frequencies for urban rail transit. Comput. Aided Civ. Inf. Eng. 32, 713–726.
Zou, C., Wang, Y.M., Wang, P., et al., 2015. Measurement of ground and nearby building vibration and noise induced by trains in a metro depot. Sci. Total Environ. 536, 761–773.
Zou, C., Wang, Y.M., Moore, J.A., et al., 2017. Train-induced field vibration measurements of ground and over-track buildings. Sci. Total Environ. 575, 1339–1351.